Effect of Geometry on Airfoil Icing Characteristics

Michael B Bragg*
Ohio State University, Columbus, Ohio

A droplet trajectory computer code is used to predict the water droplet impingement characteristics of several low and medium speed airfoils The maximum impingement efficiency, total collection efficiency, and limits of impingement are analyzed as functions of the airfoil geometry and freestream conditions The airfoil geometry is represented by leading edge radius, maximum thickness, maximum camber, and angle of attack The analysis shows that the primary effects are an increase in maximum impingement efficiency with a decrease in leading edge radius, a reduction in total collection efficiency for thicker airfoils, and a change in the limits of im pingement for airfoils of different maximum camber

Nomenclature

c = airfoil chord length, m
C_D = droplet drag coefficient, dimensionless
C_ℓ = airfoil lift coefficient, dimensionless
C_{ℓ_α} = airfoil lift curve slope, $dC_\ell/d\alpha$ per deg
E = total aii foil collection efficiency Eq (7) dimen sionless
h = airfoil projected height chords
K = inertia parameter, Eq (2), dimensionless
$\bar{K}$ = trajectory scaling parameter, Eq (5)
K_0 = modified inertia parameter, Eq (4), dimensionless
R = droplet Reynolds number, dimensionless
R_U = droplet freestream Reynolds number, Eq (3), dimensionless
r = airfoil leading edge radius of curvature, percent choi d
S_L = airfoil lower surface arc length limit of im pingement, chords
S_u = airfoil upper surface arc length limit of im pingement, chords
t = time s
U = freestream velocity, m/s
u v = droplet velocity in the x y direction, dimensionless with respect to U
x y = droplet position, chords
Δy_0 = difference between y_0's of tangent trajectories, chords
α = airfoil angle of attack deg
α_{LO} = angle of attack for zero lift, deg
β = impingement efficiency Eq (8), dimensionless
δ = droplet diameter, m
μ = absolute air viscosity, kg/m s
ρ = air density, kg/m^3
σ = droplet density, kg/m^3
τ = nondimensional time, Ut/c, dimensionless

Superscripts

$\bar{(\ )}$ = vector notation
$(\ )'$ = derivative with respect to τ

Subscripts

$(\ )_0$ = initial condition

Received Oct 25 1983

*Assistant Professor Department of Aeronautical and Astronauti cal Engineering Member AIAA

Introduction

EARLY NACA researchers were very successful in using experimental techniques to study airfoil icing and develop deicing systems However, their analytical efforts were greatly hampered by the lack of good high speed computers and flowfield algorithms Based largely on the pioneering work of Langmuir and Blodgett [1] NACA performed droplet trajectory calculations in the 1940's and 1950's for cylin ders[2,3] and Joukowski airfoils [4,5] This was, of course due to the availability of a closed form solution for these flowfields For arbitrary airfoils, a vortex substitution method was used to generate the flowfield for the droplet trajectory calculations [6-9] The computational limitations which ham pered early researchers are gone, and droplet trajectory calculations can now be made relatively quickly and ef ficiently [10,11]

This paper is based on an extensive study[12] and detailed analysis[13] of the droplet impingement characteristics of 30 low and medium speed airfoils The research effort funded by NASA Lewis Research Center, was conducted to demonstrate the fundamental effects of airfoil design on water droplet collection efficiency characteristics and provide useful information to engineers without the time or resources to perform a specific analysis The computer program described in Refs 10 and 14 was used to generate these data

Airfoils were chosen for this analysis using two basic criteria First and most importantly, airfoils were chosen which are currently in wide use on aircraft or are new sections being proposed for future use The droplet impingement characteristics of these airfoils can be used directly in the design of deicing or anti icing systems and the prediction of icing effects on unprotected airfoils A second group of airfoils was analyzed to generate data on the effect of airfoil geometry on droplet impingement The NACA airfoil families provide a convenient way to vary thickness or camber systematically while holding other parameters constant

Using primarily the data from this second group of airfoils, the present paper investigates both the influence of the freestream conditions and airfoil geometry on droplet im pingement characteristics While the current data base is indeed large and contains the predicted droplet impingement results from thirty airfoils the data cannot be considered all inclusive For any given comparison, such as varying thickness while holding leading edge radius and camber constant, only a small subset of the airfoils satisfied the constraints Therefore care must be taken when extrapolating these results outside the data set used

Analytical Method

This section presents the theoretical methods used to analyze the water droplet impingement on airfoils Aircraft icing occurs when an aircraft flies through a cloud of supercooled water droplets These droplets impact on the aircraft and accrete to form rime or glaze ice The calculation of the impingement of droplets on an airfoil is the first step in the numerical prediction of aircraft icing

Droplet Trajectories

The water droplets of interest in the icing problem are usually in the range of 10 to 50 μ in diameter These droplets experience relative Reynolds numbers sufficiently low to ensure that the particles remain spherical in shape The concentration of water in the freestream is relatively low; therefore the flow may be considered uncoupled, and the influence of the water droplets on the flowfield ignored. Assuming that the cloud of droplets may be modelled by the volume median diameter droplet, the problem reduces to the calculation of the trajectories of a series of single spherical particles about an airfoil The droplet trajectory equation can be written in nondimensional form as

$$\ddot{x}=\frac{1}{K}\left(\frac{C_D R}{24}\right)(\bar{u}-\dot{x}) \tag{1}$$

where the forces on the droplet due to gravity pressure gradient, apparent mass, and the Bassett unsteady memory term are considered small, and are therefore neglected Here K the nondimensional inertia parameter is given by

$$K=\frac{\sigma\delta^2 U}{18c\mu} \tag{2}$$

The droplet drag coefficient appears in the Stokes Law term, $C_D R/24$, and yields the second nondimensional parameter, R_U, the freestream droplet Reynolds number where

$$R_U=\frac{\rho\delta U}{\mu} \tag{3}$$

The two similarity parameters R_U and K determine the droplet trajectory for a given flowfield and set of initial conditions

It is convenient to combine R_U and K into a single, ap proximate, similarity parameter Such a nondimensional number was derived by Langmuir and Blodgett [1] Their modified inertia parameter, K_0, required a graphical or numerical procedure to determine it knowing R_U and K Recently Bragg[15] has published a closed form solution for K_0,

$$K_0=18K\left[R_U{}^{-2/3}-\sqrt{6}R_U{}^{-1}\arctan\left(\frac{R_U{}^{1/3}}{\sqrt{6}}\right)\right] \tag{4}$$

In the analysis to follow K_0 will be used to define the icing conditions

In Ref 15, a simpler similarity parameter is presented, $\bar{K}$ where

$$\bar{K}=\frac{K}{R_U{}^{\gamma}} \tag{5}$$

For the aircraft icing case $\gamma=0$ 35 has been shown to provide good data correlation $\bar{K}$ could have been substituted for K_0 in the present analysis but was not used in data presentation to conform to the established convention However $\bar{K}$ should be used to visualize qualitatively how K_0 changes with the dimensional parameters Substituting the expression for K and R_U into Eq (5), and for simplicity assuming $\gamma=1/3$

$$\bar{K}=\frac{1}{18}\left(\frac{\sigma^3\delta^5 U}{c^3\mu^2\rho}\right)^{1/3} \tag{6}$$

Therefore Eq (6) shows the relative importance of the physical parameters in determining the droplet impingement characteristics

In solving Eq (1), the flowfield is determined using the incompressible, inviscid flowfield code by Woan [16] Research is currently underway to evaluate the impact of the in compressible assumption on the droplet trajectory data At this time a compressible code does exist which shows effects on droplet impingement due to compressibility particularly at low K_0's and high subsonic Mach numbers Unfortunately, no compressible droplet impingement data exist to verify these results

Impingement Characteristics

Input to the computer code to predict the droplet im pingement characteristics are the airfoil angle of attack R_U K, droplet initial conditions, and various program control parameters All calculations are started with the droplet five chord lengths in front of the airfoil and the droplet initially at rest with respect to the freestream Once a series of trajectory calculations has been completed and particles have missed the airfoil both above and below, the tangent trajectories are determined The tangent trajectories define the total mass impinging on the airfoil The overall impingement efficiency, E, is defined as

$$E=\frac{\Delta y_0}{h} \tag{7}$$

where Δy_0 is the dimensionless distance between the y_0 values for the tangent trajectories and h is the projected height of the airfoil in chords The computer code iterates to find the tangent trajectories such that the maximum error in E never exceeds 2% of the particular value of E reported

Impingement points on the airfoil surface are reported in terms of S, the surface arc length from the leading edge Here the airfoil leading edge, $S=0$ is defined to be at the minimum x airfoil coordinate, with S positive on the upper surface and negative on the lower surface The upper and lower limits of impingement, S_u and S_L are where the tangent trajectories intersect the airfoil and thus define the area of the airfoil where water impinges

By using the droplet trajectory data, the mass flux of water impinging on the airfoil at a given S location can be deter mined The local impingement efficiency β is defined as

$$\beta=\frac{\mathrm{d}y_o}{\mathrm{d}S} \tag{8}$$

where β is the mass flux of water striking the airfoil surface nondimensionalized by that in the freestream β is obtained in the program by curve fitting the trajectory results of Y_0 vs S using a cubic spline routine The values of β and the maximum local droplet impingement $\beta_{\max}$, can be deter mined from the first derivative of the spline fit Note that the β's generated assume that the cloud is monodisperse that is, all droplets have a diameter equal to the volume median diameter

Computer Code Validation

The present method has been compared to experiment and other analytical methods to document its accuracy [10] In Fig 1 the present method is compared to experimental droplet impingement data[17] on a NACA 65_1-212 airfoil The analytical results shown are for matched C_ℓ, using the volume median diameter (VMD) droplet to simulate the actual distribution of droplet diameters The theory compares well to the experimental data The small discrepancies in the predicted β curve of reduced limits of impingement and overprediction of β_{max} are attributed to the VMD ap proximation and can be improved by modelling the distribution [10] The theory falls well within the experimental error of $\pm 10\%$ in β reported

Results and Discussion

For a given airfoil geometry, the droplet impingement characteristics are a function only of the freestream parameters, represented by K_0, and the airfoil angle of attack (or equivalently the section lift coefficient) Note that the present analysis uses an incompressible, inviscid flowfield and therefore Mach number and airfoil Reynolds number are not considered The section lift coefficient, C_ℓ, and the modified inertia parameter, K_0 are then the independent variables in the analysis When studying the effect of airfoil geometry on droplet impingement a range of C_ℓ's and K_0's must be on sidered to document the entire range of possible icing con ditions adequately In this section, first the general trends which occur with K_0 and α are described, then the additional variable of airfoil geometry is considered

Flowfield Effects

In Figs 2 through 5 the droplet impingement characteristics of a NACA 0012 airfoil are presented as a function of the flowfield variables K_0 and α The effect of K_0 on the local impingement efficiency β, is shown in Fig 2 Note from Eq (6) that like K, K_0 is a strong function of droplet diameter and airfoil chord length Therefore, increasing K_0 corresponds to increasing the droplet diameter or decreasing the airfoil chord Since K_0 represents the droplet inertia, increasing K_0 increases the droplet impingement as the droplet becomes less influenced by the airfoil flowfield All the droplet im pingement data are available from the β curve; E is the area under the curve divided by h β_{max} is the maximum β, and S_u and S_L the points on the curve where $\beta=0$ In general in creasing angle of attack moves the accretion to the lower surface, greatly affecting S_u and S_L The area under the curve increases but since E is nondimensionalized by h E changes little with α as shown in Fig 3

In Fig 3 E is almost independent of α in the range $0\le\alpha\le4$ but varies greatly with K_0 As K_0 approaches in finity, E approaches one, that is, the airfoil collects all the droplets in its projected height h Care must be taken when interpreting E Since E is nondimensionalized by h, it is a collection efficiency not a direct measure of the total amount of water impingement β_{max} vs K_0, Fig 4, is also relatively independent of α for the α's shown and strongly dependent on K_0 For large angles of attack β_{max} deviates from these curves Since as K_0 approaches infinity β becomes just the sine of the surface slope β_{max} approaches 1 0 for closed airfoil shapes

The lower surface limits of impingement for the 0012 airfoil are shown in Fig 5 Note that since the airfoil is symmetric, $S_u=-S_L$ where the angle of attack for S_u is minus that for S_L Here α and K_0 both play an important role in determining the limits Both S_u and S_L increase in magnitude with increasing K_0, and as K_0 approaches infinity, the limits asymptotically approach the points where the

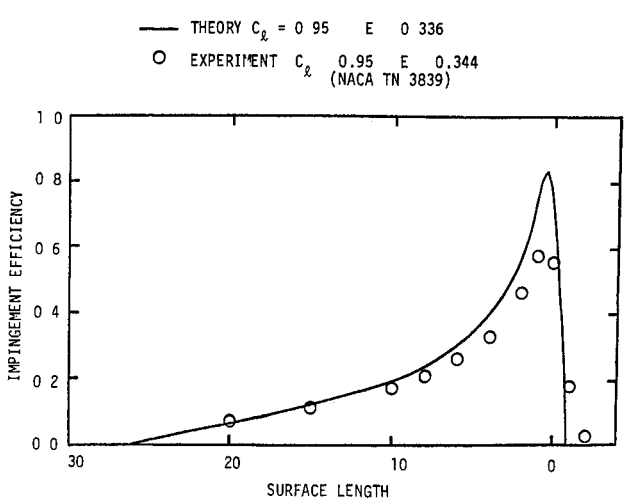

Fig. 1 Predicted and measured droplet impingement data on a NACA 65_1-212 airfoil

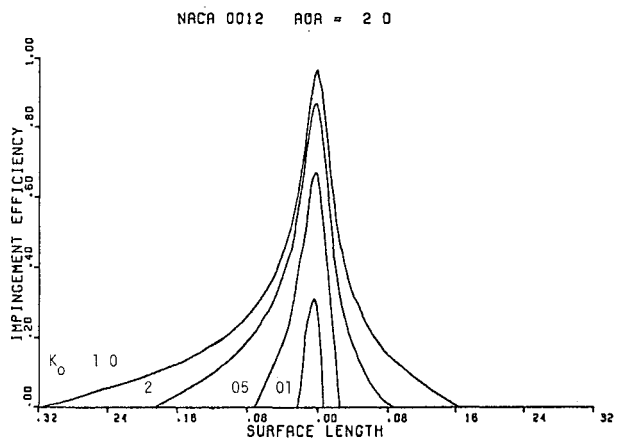

Fig 2 Impingement efficiency as a function of K_0 for a NACA 0012 airfoil at $\alpha=2$ deg

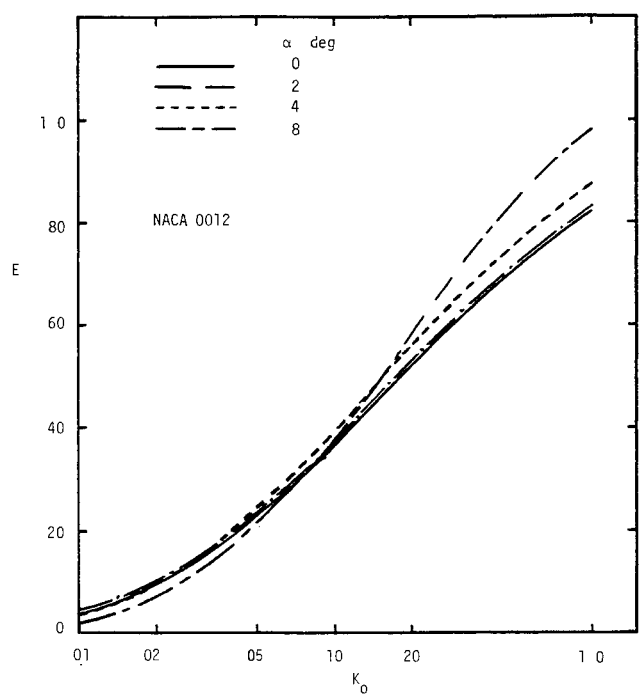

Fig 3 Collection efficiency of a NACA 0012 airfoil

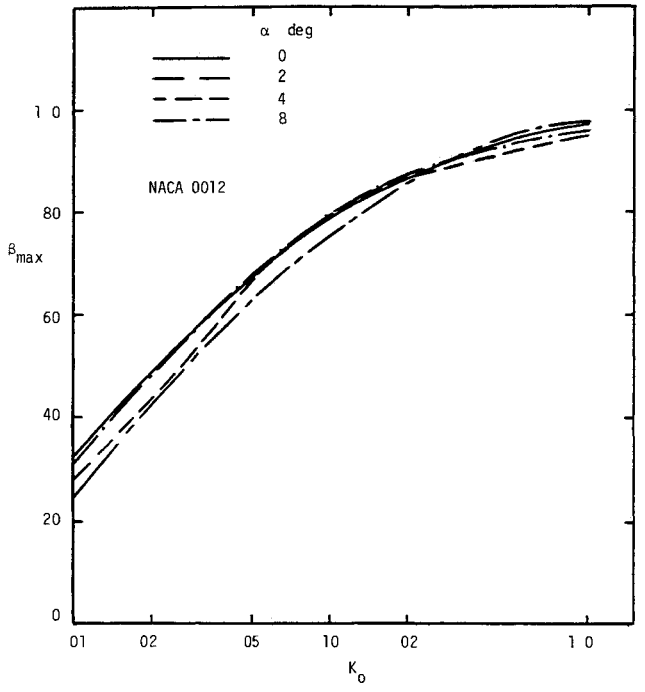

Fig 4 Maximum impingement efficiency of a NACA 0012 airfoil

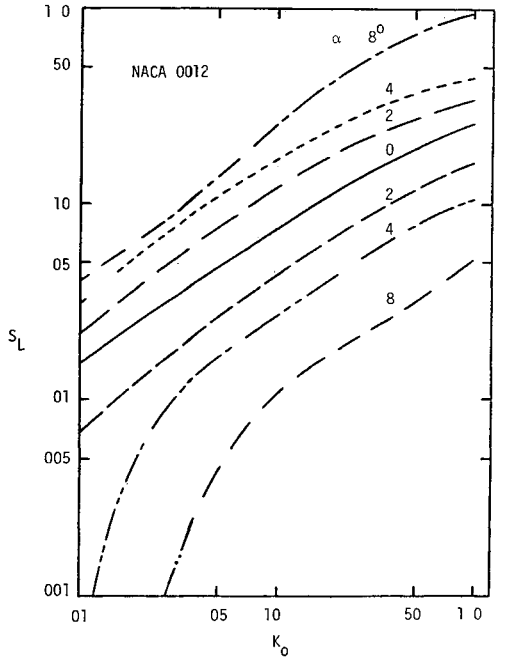

Fig 5 Lower surface limit of impingement for a NACA 0012 airfoil

surface slope on the rotated airfoil is zero As α increases the impingement moves to the lower surface, decreasing S_u and increasing the magnitude of S_L

Airfoil Geometry

For a given airfoil geometry, K_0 is seen to be the dominant parameter in determining the droplet impingement charac teristics Unfortunately the aircraft designer has control over K_0 only through the chord length, c, and this is usually fixed early in the design due to other considerations Once the planform is fixed, α is coupled to the flight velocity and becomes an operational parameter Therefore the actual airfoil geometry, within certain structural constraints is the designer's only real tool in controlling the icing characteristics

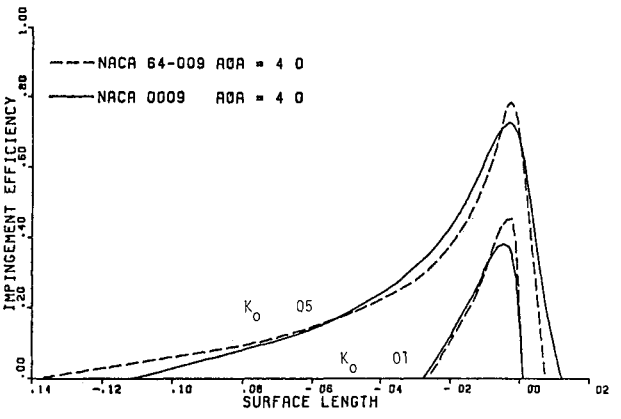

Fig 6 Effect of leading edge radius on impingement efficiency

of an unprotected wing The airfoil geometry is classified by leading edge radius, maximum thickness and maximum camber Here the influence of these on the impingement characteristics is investigated For the purposes of this comparison, the position of the maximum thickness or camber, or their actual chordwise distributions is not con sidered

Leading Edge Radius

Due to the relationship between maximum thickness and leading edge radius only the NACA 0009 and 64 009 from the airfoils analyzed match thickness and camber while having different leading edge radii In Fig 6, the β distributions at 4 deg angle of attack and for two K_0's are shown The NACA 64 009 airfoil with a leading edge radius, r, of 0 58% chord has a significantly larger β_{max} then the NACA 0009 with $r=0$ 89% chord Note also that as K_0 increases, the change in β_{max} decreases, since as K_0 approaches infinity, $\beta_{max}=1$ for both airfoils

A composite plot of several airfoils showing β_{max} as a function of leading edge radius is given in Fig 7 β_{max} is plotted for the $\alpha=4$ deg case for K_0's of 0 01, 0 05, and 1 0 Note the strong inverse relationship between β_{max} and r for values of r up to 2 0% chord and for low K_0 For r's greater than 2 0% β_{max} is approximately constant, at least up to the maximum leading edge radius of about 3 5 shown This relationship between β_{max} and r becomes less significant as K_0 increases where the droplet inertia is large and β_{max} ap proaches 1 0 for all cases The relationship between β_{max} and r shown in Fig 7 is particularly significant considering that thickness and camber are not constant here Airfoils are shown with thickness of nine to 20% and with maximum cambers from 0 7% chord The effect of r on β_{max} occurs even at relatively large α but diminishes as the location of β_{max} on the surface moves away from the leading edge

The influence of leading edge radius on collection ef ficiency E and the limits of impingement S_u and S_L do not appear to be significant Some effect is seen for very low K_0 and low α where the impingement is located almost entirely at the leading edge However the present data are insufficient to document this trend

Thickness

Thickness has its most important effect on E the overall collection efficiency In Fig 8, E is plotted as a function of airfoil thickness, with $\alpha=4$ deg for four different K_0's Airfoils from nine to 20% thick are shown regardless of their leading edge radius or camber A strong relationship is seen between E and thickness; as maximum thickness increases the overall collection efficiency decreases The slope of the curve reaches its maximum somewhere between $K_0=0$ 05 and 1 0, since the slope is zero at both $K_0=0$ and infinity where E is a constant The scatter in the data are due in part to the in

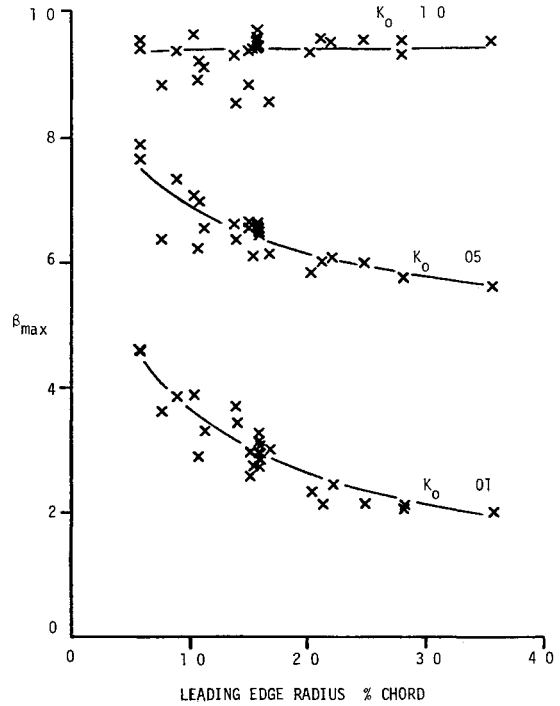

Fig 7 Maximum impingement efficiency as a function of leading edge radius at $\alpha = 4$ deg

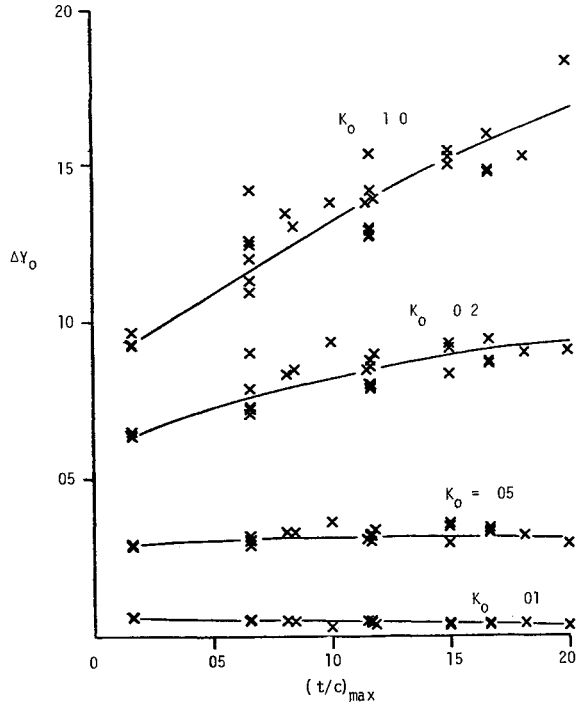

Fig 9 Effect of airfoil thickness on the total mass of water im pingement at $\alpha = 4$ deg

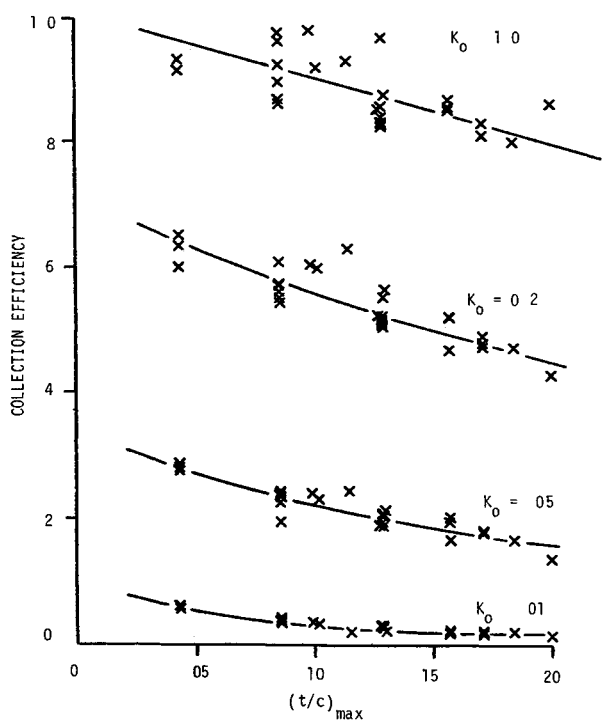

Fig 8 Airfoil thickness effects on collection efficiency at $\alpha = 4$ deg

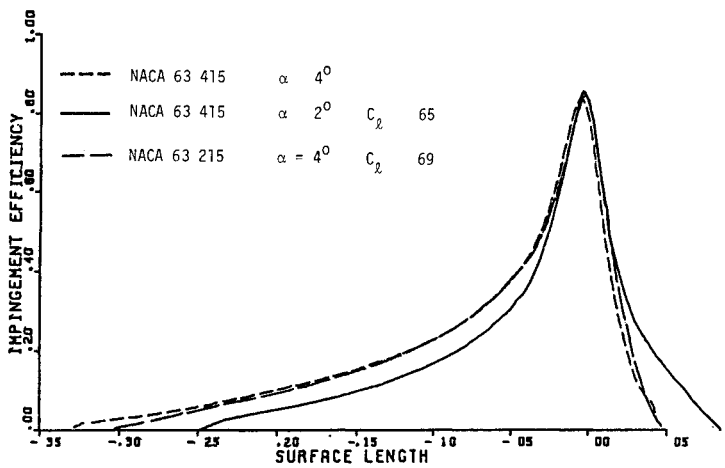

Fig 10 Effect of camber on impingement efficiency with matched α and C_ℓ

fluences of other effects such as leading edge radius and camber on E Note that at larger angles of attack, h is primarily a function of α and thickness effects will be less significant

It is important to note that while E decreases with $(t/c)_{max}$, this does not necessarily mean that thin airfoils collect more ice The total mass of droplets impinging on the airfoil, represented by Δy_0, is shown as a function of $(t/c)_{max}$ in Fig 9 for the same conditions as in Fig 8 The effect of maximum thickness on Δy_0 is exactly the opposite of E The total mass of droplets impinging on an airfoil actually increases due to increasing airfoil thickness This discrepancy is, of course due to the airfoil projected height, h, which increases with $(t/c)_{max}$ Therefore, as airfoil thickness increases, the total mass of water collected increases but the overall collection efficiency, E decreases due to the influence of the larger projected height, h This difference between E and Δy_0 is important when the weight of the ice accreted must be con sidered

Maximum thickness has little effect on β_{max} For two airfoils of the same leading edge radius but different thicknesses, β_{max} is essentially constant The limits of im pingement, S_u and S_L, show little effect of maximum thickness for low and moderate values of K_0 Here the limits are near the leading edge and more a function of leading edge geometry For large K_0 and low to moderate angle of attack maximum thickness can influence the limits of impingement However here the important parameter is the location of maximum thickness since the limits tend to approach this

value of x. When the airfoil is rotated to higher angles of attack at a large K_0, eventually the lower limit, S_L, jumps to the trailing edge. This occurs at a lower C_ℓ for thinner airfoils.

Camber

Camber affects droplet impingement differently depending if C_ℓ or α is matched between airfoils of similar thickness and leading edge radius. Figure 10 shows the NACA 63-215 and 63-415 airfoil's β curves at matched c_ℓ and α with $K_0 = 0.20$. The maximum camber for the 63-415 is exactly twice that for the 63-215 airfoil. With matched C_ℓ, a large effect on the limits of impingement due to camber is seen. In general, camber appears to move the impingement toward the upper surface. With α's constant, the β curves are very similar. No large differences between the curves are seen.

Perhaps the most significant effect of camber is on the limits of impingement, S_u and S_L In Fig. 11, S_u is shown as a function of C_ℓ for NACA 63-415 airfoils at four K_o's The trends are very clear; at constant C_ℓ, S_u increases as camber increases and except for very low K_o's, S_u is independent of camber at constant angle of attack. Since as the airfoil is cambered, the angle of attack to achieve the same lift decreases, more of the upper surface is exposed to the incoming droplets, and S_u increases. A similar effect is seen on S_L in Fig. 12. In general, S_L increases in magnitude due to a decrease in camber, and therefore an increase in α to maintain constant C_ℓ. Camber does not affect S_L for constant α just as it did not affect S_u.

The effect of camber on S_L is sometimes reversed for relatively high K_0's and C_ℓ's when droplets impinge on the entire lower surface. The more highly cambered airfoils are the first to have droplets impinge on the entire lower surface as C_ℓ is increased. This rapid increase in S_L is sometimes due to a small droplet impingement on the very aft portion of the airfoil lower surface due to the effective flap caused by the airfoil camber. The effect of camber on S_u and S_L occurs throughout the airfoils analyzed and therefore appears to be a general result.

The effect of camber on β_{max} is not significant. As discussed earlier, only leading radius appears to affect β_{max} significantly Camber does affect collection efficiency E, but it is a very complex relationship. Holding α constant, h increases with increased camber, and the effects on Δy_0 and E generally follow However, for matched C_ℓ, the effects are more complex.

Noting the change in h with camber and C_ℓ helps explain the trends in E. At high C_ℓ's, decreasing camber increases h as the less cambered airfoils must be rotated to a higher α. The reverse is true at low C_ℓ where to obtain a small C_ℓ the cambered airfoils must be rotated to larger negative α's, increasing h. The minimum h for each airfoil occurs at higher C_ℓ's as camber is increased. For cambered airfoils this occurs at C_ℓ's slightly above the design C_ℓ depending on camber and thickness distribution.

The trends in Δy_0 with camber are very similar to those for h, with the exact magnitude of the effects a function of K_0. E also is affected by camber in a similar manner as h, At low K_0, the effect is small as E approaches zero for all airfoils. At high C_ℓ the effect of camber on E decreases as the high angle of attack dominates. These effects of camber on h, Δy_0, and E are complex and can be easily masked or confused by changes in other parameters, including thickness and camber distribution effects on h.

New Airfoil Sections

Ten airfoils were analyzed which were considered representative of the new laminar and turbulent sections designed in the 1970's and 1980's.[12] These airfoils usually were not suitable for the earlier comparisons, since they seldom matched the NACA sections in leading edge radius, thickness, or camber. To ascertain if these airfoils have droplet impinge

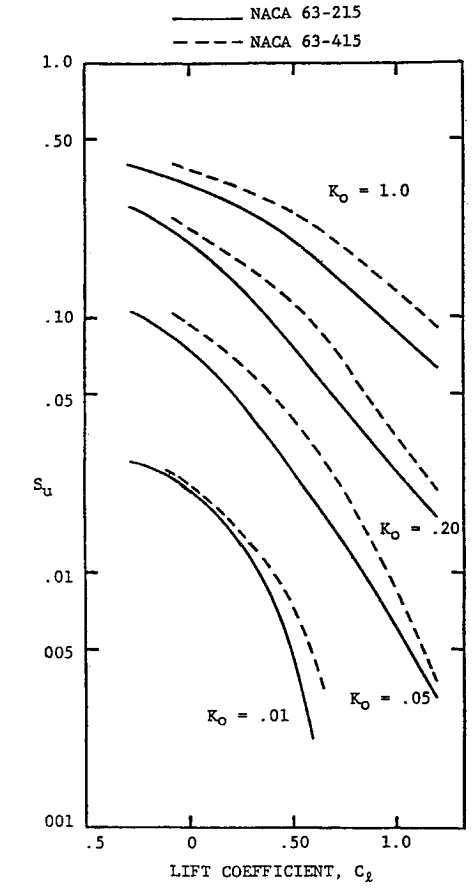

Fig. 11 Effect of camber on the upper surface limit of impingement as a function of C_ℓ.

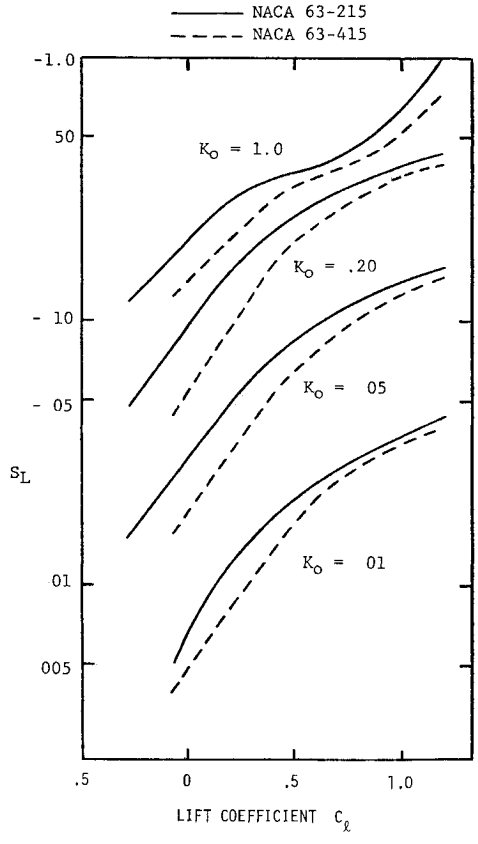

Fig. 12 Effect of camber on the lower surface limit of impingement as a function of C_ℓ.

ment characteristics significantly different than the NACA sections, four airfoils were considered: the Wortman FX 67 K 170/17, NASA MS(1) 0317 NASA GA(W) 2, and OSU NLF 0315 These airfoils were compared to NACA sections of similar geometry with respect to their droplet impingement characteristics

In comparison to the NACA airfoils the newer sections appear to follow the same trends in droplet impingement as a function of airfoil geometry No significant discrepancy was observed for the four newer airfoils used in the comparison Some sections, however such as the Wortman section represent combinations of camber and thickness outside the NACA airfoil data base While the general trends appear consistent, it is difficult to make more specific comparisons without airfoil impingement data on similar NACA airfoils

Summary and Conclusions

The droplet impingement characteristics of thirty low and medium speed airfoils have been analyzed to determine the effect of the freestream parameters and airfoil geometry on droplet impingement The data base included airfoils from the NACA four and five digit series as well as the six series airfoils Several of the newer airfoils such as the GAW series and new laminar flow airfoils, were also included Freestream parameters K_0 and α (or C_ℓ) and airfoil geometry variables of leading edge radius, maximum thickness, and maximum camber were studied as they influence droplet impingement as documented by β_{max}, E S_u and S_L

The effect of freestream parameters K_0 and α are seen to have large effects on droplet impingement As K_0 increases impingement increases and E β_{max}, S_u, and the magnitude of S_L also increase K_0 determines the relative importance of the inertia and drag forces and is the single most important parameter in determining collection efficiency characteristics The angle of attack governs the position of the droplet impingement on the airfoil: as α increases S_u decreases and the magnitude of S_L increases While E is nondimensionalized to remove α effects, the total mass of droplets impinging on the airfoil increases as α increases.

The primary purpose of this study was to determine the lesser known effects of airfoil geometry on droplet impingement While several lesser effects have been noted, the primary airfoil geometry effects are: 1) β_{max} increases with decreasing leading edge radius, 2) increasing maximum thickness decreases E due to the change in airfoil projected height with thickness, and 3) increasing maximum camber while holding C_ℓ constant increases S_u and decreases the magnitude of S_L

In studying the newer airfoils, no significant differences were seen as compared to the NACA airfoils They appear to follow the same trends with respect to leading edge radius thickness, and camber

By expanding the current data bank of airfoils tested additional parameters could be studied which were beyond the scope of this research Thickness and camber were documented using their maximum values only The chordwise distribution of camber and thickness probably affects S_u and S_L and may influence other impingement parameters Future studies should consider these more detailed effects In the current study, the droplet impingement parameters considered did not include the details of the shape of the β curves It is the β curve, along with the thermodynamics, which actually determines the ice accretion shape Documenting the more detailed changes in β with airfoil geometry may provide some insight into the ice accretion problem Finally, the most useful information for unprotected airfoils would be the change in airfoil aerodynamic performance due to icing as a function of airfoil geometry While performing these calculations is currently beyond the capabilities of computational methods, it is hoped that current research will lay the foundation for such methods

Acknowledgment

The bulk of the work involved in running the computer programs and plotting the results for this paper was ably performed by Stan Cosstephens and Steve Thompson, undergraduate research assistants at the Aeronautical and Astronautical Research Laboratory This work was supported by NASA Lewis Research Center under Grant NAG 3 28 The author is indebted to Dr R J Shaw of NASA Lewis for his guidance during the project

References

[1]Langmuir I and Blodgett K B A Mathematical Investigation of Water Droplet Trajectories ' Army Air Forces Technical Report No 5418 Contract No w 33 038 ac 9151 Feb 1946

[2]Brun R J. Serafini J S , and Gallagher H M , ' Impingement of Cloud Droplets on Aerodynamic Bodies as Affected by Compressibility of AIr Flow Around the Body ' NACA TN 2903 March 1953

[3]Brun R J and Mergler H W Impingement of Water Droplets on a Cylinder in an Incompressible Flow Field and Evaluation of Rotating Multicylinder Method for Measurement of Droplet Size Distribution Volume Median Droplet Size, and Liquid Water Content in Clouds NACA TN 2904 March 1953

[4]Bergrun N R , A Method for Numerically Calculating the Area and Distribution of Water Impingement on the Leading Edge of an Airfoil in a Cloud NACA TN 1397 Aug 1947

[5]Brun R J and Vogt D E Impingement of Cloud Droplets on 36 5 Percent Thick Joukowski Airfoil at Zero Angle of Attack and DIscussion of Use as Cloud Measuring Instrument in Dye Tracer Technique NACA TN 4035 Sept 1957

[6]Brun R J. Gallagher H M , and Vogt D E Impingement of Water Droplets on NACA 65 208 and 65 212 Airfoils at 4 Angle of Attack NACA TN 2952 May 1953

[7]Brun R J Gallagher H M , and Vogt D E ' Impingement of Water Droplets on NACA 65A004 Airfoil and Effects of Change in Airfoil Thickness from 12 to 4 Percent at 4 Angle of Attack ' NACA TN 3047 Nov 1953

[8]Brun R J , Gallagher, H M and Vogt D E Impingement of Water Droplets on NACA 65A004 Airfoil at 8 Angle of Attack NACA TN 3155 July 1954

[9]Brun R J and Vogt D E. Impingement of Water Droplets on NACA 65A004 Airfoil at 0 Angle of Attack NACA TN 3586 Nov 1955

[10]Bragg M B , Rime Ice Accretion and Its Effect on Airfoil Performance Ph D dissertation, The Ohio State University Columbus Oh , 1981 and NASA CR 165599 1982

[11]Lozowski E P and Oleskiw, M M Computer Simulation of Airfoil Icing Without Runback, AIAA Paper No 81 0402 presented at the 19th Aerospace Sciences Meeting St Louis Mo Jan. 12 15 1981

[12]Bragg M B and Gregorek G M An Incompressible Droplet Impingement Analysis of Thirty Low and Medium Speed Airfoils ' to be published as NASA CR

[13]Bragg M B and Gregorek, G M An Analytical Evaluation of the Icing Properties of Several Low and Medium Speed Airfoils AIAA Paper No 83 109 presented at the 21st Aerospace Sciences Meeting Reno Nev Jan 10 13 1983

[14]Bragg M B , Gregorek G M and Shaw R J , An Analytical Approach to Airfoil Icing AIAA Paper No 81 0403, presented at the 19th Aerospace Sciences Meeting St Louis Mo Jan 12 15 1981

[15]Bragg M B A Similarity Analysis of the Droplet Trajectory Equation *AIAA Journal* Vol. 20, Dec 1982 pp 1681 1686

[16]Woan C J Fortran Programs for Calculating the Incompressible Potential Flow ABout a Single Element Airfoil Using Conformal Mapping The Ohio State University Aeronautical and Astronautical Research Laboratory TR AARL 80 02 Jan 1980

[17]Gelder T F Smyers W H Jr and Von Glahn U H , Experimental Droplet Impingement on Several Two Dimensional Airfoils with Thickness Ratios of 6 to 16 Percent NACA TN 3839 Dec 1955